

Non-Schwarzschild black holes sourced by scalar-vector fields

Manuel Gonzalez-Espinoza ^{1,*} Y. Gómez-Leyton,^{2,†} Z. Stuchlik,^{3,‡} and Francisco Tello-Ortiz ^{4,§}

¹*Instituto de Física, Pontificia Universidad Católica de Valparaíso, Casilla 4950, Valparaíso, Chile*

²*Departamento de Física, Universidad Católica del Norte, Av. Angamos 0610, Antofagasta, Chile.*

³*Research Centre for Theoretical Physics and Astrophysics, Institute of Physics,
Silesian University in Opava, Bezručovo nám. 13, 74601 Opava, CZ*

⁴*Departamento de Ciencias Físicas, Universidad de La Frontera, Casilla 54-D, 4811186 Temuco, Chile.*

In a scalar-vector-gravity theory with the vector sector described by nonlinear electrodynamics, the field equations are integrated using the well-known gravitational decoupling method. The resulting spacetime corresponds to a spherically symmetric and static non-Schwarzschild black hole. Employing the master equations for both even and odd parity modes, it is proven that the solution is stable under certain conditions satisfied by the scalar and vector field parameters. To further corroborate the theoretical feasibility of this toy model, the causal structure, geodesic motion for massive particles, and some thermodynamic features are analyzed in detail.

I. INTRODUCTION

The theoretical and observational study of black holes (BHs) continues to be a cornerstone of modern gravitational physics. Over the past decade, the field has experienced an unprecedented renaissance driven by two major developments: the direct detection of gravitational waves from compact binary coalescence by LIGO–Virgo–KAGRA [1, 2], and the imaging of supermassive BH shadows by the Event Horizon Telescope (EHT) [3–5]. These advances have opened new avenues for testing the strong-field predictions of general relativity (GR) and for probing possible signatures of additional fields or new gravitational degrees of freedom.

From a theoretical perspective, there is a longstanding interest in black hole solutions supported by scalar, vector, or non-linear electrodynamic fields. Such matter sectors arise naturally in effective field theories beyond GR, including low-energy string-inspired models [6, 7], generalized Proca theories [8, 9], non-linear electrodynamics [10, 11], and scalar–vector–tensor extensions [12, 13]. These constructions provide a rich framework to explore phenomena such as modified horizon geometries, deviations in geodesic motion, new stability channels, and non-standard thermodynamics. However, obtaining exact and physically well-behaved solutions, particularly those preserving asymptotic flatness and a single horizon, remains a highly non-trivial task.

The gravitational decoupling (GD) program, and specifically its Minimal Geometric Deformation (MGD) formulation introduced in [14], offers an elegant and systematic approach for constructing new solutions to the Einstein equations by deforming a known “seed” geometry. In this framework, the total energy–momentum tensor is decomposed into a seed sector and an auxiliary

“decoupling” contribution, with the deformation encoded directly in the metric. A key feature of the MGD method is the possibility of implementing *minimal* deformations, where the temporal metric component is preserved, and only the radial part receives a correction. This ensures that many geometric properties of the seed solution, including its causal structure and asymptotic behavior, are maintained while still allowing for non-trivial modifications induced by additional matter sources. This approach has been widely applied in the context of BHs physics [15–42], demonstrating its versatility.

BHs impose stricter geometric and physical requirements, such as the preservation of a consistent Lorentzian signature, the existence of a unique event horizon, and compatibility with perturbative stability conditions. These constraints make the development of minimally deformed BHs particularly appealing: such solutions maintain the essential structure of a classical BH while incorporating the influence of additional fields in a controlled and analytically tractable manner. Moreover, minimally deformed BHs offer a clean theoretical setting for examining how new matter sectors modify observable quantities such as orbital precession, lensing, quasinormal spectra, or thermodynamic relations, without altering the overall causal framework.

In the present work, we construct a static and spherically symmetric BH solution sourced by a non-linear scalar–vector sector and generated through the MGD approach. The resulting geometry preserves the temporal metric component of the Schwarzschild solution and introduces a well-defined deformation exclusively in the radial sector. To our knowledge, this represents one of the first explicit instances in which a minimally deformed extension of Schwarzschild leads unambiguously to a single-horizon, asymptotically flat, and physically interpretable BH supported by a non-linear scalar–vector interaction. This provides a new analytical laboratory to explore the interplay between geometric deformations, non-linear matter fields, and classical BH phenomenology, and contributes to the broader effort of extending GR solutions using the GD methodology.

The article is organized as follows: Sect. II revisited

* manuel.gonzalez@pucv.cl

† y.gomez@ucn.cl

‡ zdenek.stuchlik@fpf.slu.cz

§ francisco.tello@ufrontera.cl

GD by MGD in short. Sect. III introduces the model, its causal structure, reconstruction of the matter sector, and stability analysis via odd and even parity master constraints. Then, Sect. IV presents the geodesic motion study for massive particles and Sect. V is devoted to the thermodynamic study. Finally, Sect. VI concludes the work.

In this work the mostly positive signature $\{-, +, +, +\}$ is used and units where $c = G = 1$.

II. GRAVITATIONAL DECOUPLING IN SHORT

Here we introduce the main aspect to be used in the context of the well-known GD by MGD approach [14, 43]. The main point is to consider an extended energy-momentum tensor, composed by two sources. Explicitly this reads

$$T_{\mu\nu} \equiv \tilde{T}_{\mu\nu} + \alpha\theta_{\mu\nu}, \quad (1)$$

where $\tilde{T}_{\mu\nu}$ is known as the seed source and $\theta_{\mu\nu}$ an extra unknown source which introduces new physical content beyond the given by the seed matter.

In canonical coordinates, the space-time metric of a spherically symmetric and static spacetime, is given by

$$ds^2 = -e^\nu dt^2 + e^\lambda dr^2 + r^2 d\Omega^2, \quad (2)$$

with $d\Omega^2 \equiv d\theta^2 + \sin^2\theta d\phi^2$ the usual line element of a unitary two sphere and ν and λ are functions of the radial coordinate only. Taking into account that this general line element in (2) solves the Einstein field equations ¹

$$G_{\mu\nu} \equiv R_{\mu\nu} - \frac{1}{2}g_{\mu\nu}R = -8\pi T_{\mu\nu}, \quad (3)$$

one arrives at

$$8\pi\rho = \frac{1}{r^2} - e^{-\lambda} \left(\frac{1}{r^2} - \frac{\lambda'}{r} \right), \quad (4)$$

$$8\pi p_r = -\frac{1}{r^2} + e^{-\lambda} \left(\frac{1}{r^2} + \frac{\nu'}{r} \right), \quad (5)$$

$$8\pi p_\perp = \frac{1}{4}e^{-\lambda} \left(2\nu'' + \nu'^2 - \lambda'\nu' + 2\frac{\nu' - \lambda'}{r} \right), \quad (6)$$

where primes denote derivation with respect to the radial coordinate, r , and the quantities $\{\rho, p_r, p_\perp\}$ refer to the density and to the radial and transverse pressures, respectively.

In the framework of GD, we assume that the energy-momentum tensor can be written as a linear combination of different fluids, namely

$$T_{\mu\nu} \equiv \tilde{T}_{\mu\nu} + \theta_{\mu\nu}, \quad (7)$$

where $\tilde{T}_{\mu\nu} = \text{diag}\{\tilde{\rho}, -\tilde{p}_r, -\tilde{p}_\perp, -\tilde{p}_\perp\}$ is a known source, the so-called seed energy-momentum tensor, $\theta_\mu^\nu = \text{diag}\{\theta_0^0, \theta_1^1, \theta_2^2, \theta_3^3\}$ is a certain unknown generic fluid, the so-called decoupling fluid, and α is a free parameter we introduce to regulate the impact of the generic fluid on the seed. Next, after implementing the following splitting in the metric potentials

$$\nu = \xi + \alpha g \quad (8)$$

$$e^{-\lambda} = \mu + \alpha f, \quad (9)$$

the system (4) decouples in two set of differential equations: one for the metrics ξ and μ sourced by $\tilde{T}_{\mu\nu}$ and other for f and g sourced by $\theta_{\mu\nu}$.

In this work, we will focus on the MGD, which corresponds to setting $g = 0$ such that $g_{tt} = e^\nu$ is always the same, and all the effects coming from the decoupling-sector lie on the radial metric potential [14, 43]. Now, plugging the transformations (8) into (4)–(6) under the mentioned considerations, one gets

$$8\pi\tilde{\rho} = \frac{1}{r^2} - \frac{\mu}{r^2} - \frac{\mu'}{r}, \quad (10)$$

$$8\pi\tilde{p}_r = -\frac{1}{r^2} + \mu \left(\frac{1}{r^2} + \frac{\xi'}{r} \right), \quad (11)$$

$$8\pi\tilde{p}_\perp = \frac{\mu}{4} \left(2\xi'' + \xi'^2 + \frac{2\xi'}{r} \right) + \frac{\mu'}{4} \left(\xi' + \frac{2}{r} \right), \quad (12)$$

along with the conservation equation

$$\frac{d\tilde{p}_r}{dr} + \frac{\xi'}{2} (\tilde{\rho} + \tilde{p}_r) - \frac{2}{r} (\tilde{p}_\perp - \tilde{p}_r) = 0, \quad (13)$$

and

$$-8\pi\theta_0^0 = \alpha \frac{f}{r^2} + \alpha \frac{f'}{r}, \quad (14)$$

$$-8\pi\theta_1^1 = \alpha f \left(\frac{1}{r^2} + \frac{\xi'}{r} \right), \quad (15)$$

$$-8\pi\theta_2^2 = \frac{\alpha f}{4} \left(2\xi'' + \xi'^2 + 2\frac{\xi'}{r} \right) + \frac{\alpha f'}{4} \left(\xi' + \frac{2}{r} \right), \quad (16)$$

with

$$(\theta_1^1)' - \frac{\xi'}{2} (\theta_0^0 - \theta_1^1) - \frac{2}{r} (\theta_2^2 - \theta_1^1) = 0. \quad (17)$$

At this point, some comments are in order. First, note that Eqs. (10)–(12) solve the system when $\alpha = 0$. In this regard, this set corresponds to identities after we provide a well-known seed, $\tilde{T}_{\mu\nu}$, which could be a perfect fluid, a charged fluid, etc. Second, as the g_{tt} component of the metric is the same for each sector, the set (14)–(16) corresponds to three differential equations with four unknowns, namely $\{f, \theta_0^0, \theta_1^1, \theta_2^2\}$ so extra information is required to close the system. This condition could be, for example, a well-motivated relation among the θ -sector components (a type of equation of state), or some

¹ We are using units where $c = G = 1$

constraint on the spacetime scalar curvature, to name a few. Finally, it can be shown that both matter sectors are separately conserved, namely

$$\nabla_\mu \tilde{T}^{\mu\nu} = 0 \quad (18)$$

$$\nabla_\mu \theta^{\mu\nu} = 0, \quad (19)$$

which entails that there is no exchange of energy between them, which resembles how dark matter interacts with baryonic matter.

III. NON-SCHWARZSCHILD BLACK HOLES

As stated at the end of the previous section, to close the θ -sector, Eqs. (14)-(16), one needs to specify both the seed spacetime and an additional constraint imposed on the components of the $\theta_{\mu\nu}$ tensor. In this context, here we consider the seed solution to be the well-known Schwarzschild BH solution whose line element reads

$$ds^2 = -h dt^2 + h^{-1} dr^2 + r^2 d\Omega^2, \quad (20)$$

where

$$h = e^\xi = \mu = 1 - \frac{2M}{r}, \quad (21)$$

with M being the mass parameter. The Schwarzschild solution is Ricci flat as by the energy-momentum tensor $\tilde{T}_{\mu\nu} = 0$. Therefore, in applying the MGD protocol, we are going to obtain a non-Schwarzschild metric, that is, a spacetime having $g_{tt}g_{rr} \neq -1$. Therefore, whether this remains or not being a BH spacetime strongly depends on the additional piece usually introduced by MGD on the radial metric potential. This is so because the original causal structure could be destroyed by the appearance of new critical points, which can be coordinate or physical

singularities. Therefore, it is very relevant to endow the θ -sector with physical meaning to avoid any undesirable situation.

A. The scalar-vector action

The solution of the system (14)-(16) will be carried out by considering that the θ -sector is described by a scalar-vector interaction. The action representing this interaction is given by

$$S = \int d^4x \sqrt{-g} [X^m - F^s V(\phi)], \quad (22)$$

where, for the scalar field, we consider the kinetic term to be of the form

$$X = -\frac{1}{2} \nabla_\mu \phi \nabla^\mu \phi, \quad (23)$$

and $V(\phi)$ is a generic function depending on the scalar field. For the vector field one has

$$F = -\frac{1}{4} F_{\mu\nu} F^{\mu\nu}, \quad F_{\mu\nu} = \nabla_\mu A_\nu - \nabla_\nu A_\mu. \quad (24)$$

It is worth noting that the matter sector considered here contains two distinct contributions: a scalar kinetic term X^m and a nonlinear vector contribution $F^s V(\phi)$. In principle, the model contains both scalar and vector sectors; however, due to their coupling, they cannot be treated independently. The scalar-only case would correspond to a k-essence type source governed by the kinetic structure X^m , while the vector-only case would reduce to a non-linear electrodynamic theory. In the present work, we focus on the combined scalar-vector interaction, since such couplings naturally arise in effective field theory extensions of gravity and provide a convenient closure of the decoupling sector within the MGD framework.

Here, the exponents m and s are positive real numbers. The action (22) can be seen as a particular case of the action provided in [44], corresponding to a non-minimal coupling between scalar field and non-linear electrodynamics.

Next, the full set of equations (14)-(16) reads as follows

$$\begin{aligned} X^m + (2s-1)F^s V(\phi) &= -\frac{\alpha}{8\pi} \left[\frac{f}{r^2} + \frac{f'}{r} \right], \\ (1-2m)X^m + (2s-1)F^s V(\phi) &= -\frac{\alpha}{8\pi} f \left(\frac{1}{r^2} + \frac{\xi'}{r} \right), \\ X^m - F^s V(\phi) &= -\frac{\alpha}{8\pi} \left[\frac{f}{4} \left(2\xi'' + \xi'^2 + 2\frac{\xi'}{r} \right) + \frac{f'}{4} \left(\xi' + \frac{2}{r} \right) \right]. \end{aligned} \quad (25)$$

along with the conservation equation

$$\begin{aligned} mX^{m-1} \left[(2m-1)\phi'' + \left(\frac{2}{r} + \frac{\nu' + (1-2m)\lambda'}{2} \right) \phi' \right] \\ - e^\lambda F^s \frac{dV}{d\phi} + \frac{se^\lambda F^s V}{\phi'} \frac{d}{dr} [\ln(r^4 V^2 F^{2s-1})] = 0. \end{aligned} \quad (26)$$

Besides, the equations of motion for the scalar field and

for the vector field are

$$(2m-1)\phi'' + \left(\frac{2}{r} + \frac{\nu' + (1-2m)\lambda'}{2} \right) \phi' = \frac{1}{m} \frac{e^\lambda F^s}{X^{m-1}} \frac{dV}{d\phi}, \quad (27)$$

$$r^4 V^2 F^{2s-1} = \text{const}, \quad (28)$$

respectively. It is worth mentioning that Eqs. (27) and (28) are contained by the conservation Eq. (26). Moreover, since Eq. (26) is a linear combination of the field equations (25), so no new information can be obtained from the it, and the set (25) must be supplemented with extra information to determine $\{f, \phi, V, A_\mu\}$.

B. The metric

The closure of the θ -sector is not only subject to its identification with a well-motivated matter content, but

also it is necessary to consider some functional relation between its components, such as an equation of state (EoS). In this regard, we consider a general relation given by

$$\theta_0^0 = a\theta_1^1 + b\theta_2^2, \quad (29)$$

where a and b are positive dimensionless constants. In this way, the equation (29) provides an interesting relation among the parameters $\{a, b, s, m\}$ and the scalar and vector fields

$$(-2as + a + b + 2s - 1)F^s V(\phi) - (-1 + a + b - 2am)X^m = 0. \quad (30)$$

The above relation is valid if and only if the exponents satisfy

$$m = \frac{a+b-1}{2a}, \quad s = \frac{a+b-1}{2(a-1)}. \quad (31)$$

On the other hand, the geometric part leaves the following differential equation for the decoupler function $f(r)$

$$\frac{d \ln f(r)}{dr} = \frac{2[(2a+b-4)Mr - (a-1)r^2 - (b-4)M^2]}{[2M-r][(b-4)M - (b-2)r]r}, \quad (32)$$

leading to the following result

$$f(r) = \frac{[r-2M][(4-b)M + (b-2)r]^c}{r} l, \quad (33)$$

where

$$c \equiv \frac{2(1-a)}{(b-2)}, \quad (34)$$

and l an integration constant with units of length^{-c}.

At this point, some comments are in order. First, the decoupler function (33) contains the seed metric potential. Therefore, the full inverse radial metric component reads as follows

$$g_{rr}^{-1}(r) = \left[1 - \frac{2M}{r} \right] [1 + l\alpha(r(b-2) - (b-4)M)^c]. \quad (35)$$

In this way, the minimally deformed Schwarzschild BH is given by the following line element

$$ds^2 = - \left[1 - \frac{2M}{r} \right] dt^2 + \left[1 - \frac{2M}{r} \right]^{-1} \times [1 + l\alpha(r(b-2) - (b-4)M)^c]^{-1} dr^2 + r^2 d\Omega^2. \quad (36)$$

Now, a well established BH solution should preserve the Lorentzian signature throughout the whole spacetime. Furthermore, as we are interested in saving the

asymptotic behavior of the seed manifold, it is imperative to restrict the new information coming from the decoupler sector. To avoid changes in signature, it is necessary to ensure that no new horizons are formed after introducing the θ -sector. This is so because, once the new horizon r_H^* , provided by the condition $g_{rr}^{-1}(r) = 0$ is crossed, only the radial metric component changes sign producing the following signature $\{-, -, +, +\}$, assuming $r_H^* > 2M$. Otherwise, if $0 < r_H^* < 2M$ then, one obtains an Euclidean signature, that is, $\{+, +, +, +\}$. Therefore, in both cases, the spacetime signature is ill-defined. Then,

$$\left[1 - \frac{2M}{r} \right] [1 + l\alpha(r(b-2) - (b-4)M)^c] = 0, \quad (37)$$

provides

$$r_1 = 2M, \quad r_2 = \frac{(b-4)M + (-l\alpha)^{-1/c}}{b-2} \quad (38)$$

The condition of avoiding the introduction of an additional causal structure beyond the original is to consider $l\alpha > 0$. In such a case, the additional r_2 roots are imaginary roots. Nevertheless, as we shall see later, this condition in $l\alpha$ is not sufficient to ensure the stability of the model. Then, for negative $l\alpha$, the only chance of having just one horizon (event horizon, Killing horizon), is for those values of $l\alpha$ satisfying

$$-(4M - bM)^{-c} < l\alpha < 0, \quad (39)$$

and also for those values of parameter b satisfying

$$2 < b < 4. \quad (40)$$

Besides, as it is desirable to keep the asymptotic behavior of the seed solution, the parameter c defined by Eq. (34) should be negative in nature. This is compatible with conditions (39) and (40). In Fig. 1 it is shown the trend of the inverse radial metric potential against the radial coordinate, where it is clear that the solution has only one horizon. These restrictions guarantee that the deformation does not introduce additional real roots of the radial metric component outside the Schwarzschild horizon, thus preserving the original causal structure of the seed geometry.

Another important requirement concerns the asymptotic behavior of the spacetime. In order to preserve the asymptotic flatness of the Schwarzschild seed geometry, the deformation term must vanish at large radial distances. This condition is satisfied when the exponent c defined in Eq. (34) is negative, ensuring that the additional contribution to the radial metric component decays sufficiently fast as $r \rightarrow \infty$. Consequently, the spacetime approaches the Schwarzschild geometry asymptotically.

The above conditions define a restricted region in the parameter space where the resulting geometry represents a physically acceptable black hole spacetime. In particular, the combined requirements of asymptotic flatness, Lorentzian signature, and the absence of additional horizons constrain the parameters $(b, l\alpha)$ to lie within a finite domain. To illustrate these constraints, in Fig. 2 we display the allowed region in the $(b, l\alpha)$ parameter space for a representative choice of the exponent $c = -2$ and $M = 1$. The horizontal axis represents the parameter b , while the vertical axis corresponds to the deformation pa-

rameter $l\alpha$. The solid black line BH denotes the critical boundary

$$l\alpha_{\text{crit}}(b) = -(4-b)^2, \quad (41)$$

obtained from the condition that the second factor of the radial metric component becomes zero. This curve separates two qualitatively distinct branches of BH solutions. The blue shaded region above the curve corresponds to the *single-horizon branch*, where the only root of g_{rr}^{-1} is located at $r = 2M$, corresponding to the Schwarzschild horizon. In this region, the MGD deformation preserves the causal structure of the Schwarzschild seed geometry, and no additional horizons are generated. The red shaded region below the critical curve corresponds to the *multi-horizon branch*. In this case, the deformation term introduces an additional root of the radial metric function, producing a spacetime structure with more than one horizon. The dashed horizontal line represents $l\alpha = 0$, which corresponds to the Schwarzschild limit where the deformation vanishes. The gray region above this line corresponds to $l\alpha > 0$, which lies outside the branch considered in the present analysis. Finally, the vertical dashed lines indicate the interval (40), which follows from the conditions required to maintain the regular behavior of the deformation function and the existence of well-defined horizons.

As the field equations (25) are quite involved, it is not easy in general to determine either the scalar field or the function V , and in principle, the electromagnetic vector field cannot be easily determined either. However, in the representative branch, it can be done (see below). Now, the expression for the derivative of the scalar field is obtained by subtracting the first and second equations in the set (25). So, this provides

$$\phi'(r)^2 = -\frac{r((b-2)r - (b-4)M)^{\frac{2a}{b-2}} \left(\frac{l\alpha(a-1)2^m(2M-r)((b-2)r - (b-4)M)^{-\frac{2a+b-4}{b-2}}}{mr^2} \right)^{1/m}}{(r-2M) \left(((b-2)r - (b-4)M)^{\frac{2a}{b-2}} + l\alpha((b-2)r - (b-4)M)^{\frac{2}{b-2}} \right)}. \quad (42)$$

The above expression blows up at the event horizon. Therefore, to avoid any pathological behavior, we shall

consider $m = 1$. Now, using the third equation of (25), one obtains

$$-sF^{s-1}V(\phi) = \alpha \frac{2^{\frac{a+b-1}{2(a-1)}}((b-2)r - (b-4)M)^{\frac{2}{b-2}-1}(M(-3a+b-1) + r(a-b+1))}{r^2 A_0'^2 \left(((b-2)r - (b-4)M)^{\frac{2a}{b-2}} + l\alpha((b-2)r - (b-4)M)^{\frac{2}{b-2}} \right)}. \quad (43)$$

As can be observed, the previous expression depends on A_0' , that is, the derivative of the temporal component of the four-potential A_μ . This comes from the spheri-

cal and static features of the model, where there is only one non-trivial component. In connection with the vector field equation (28), in principle it can be formally inte-

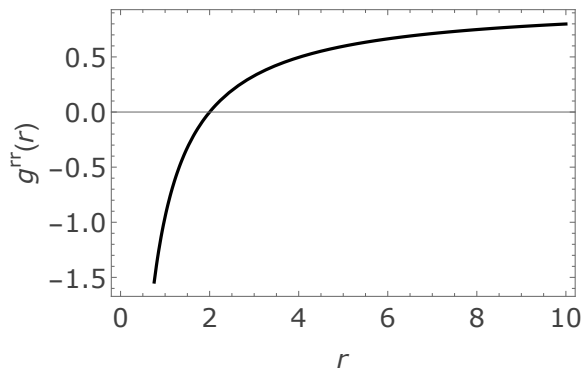


FIG. 1. The inverse radial metric potential versus the radial coordinate for $M = 1$, $b = 3$, $c = -2$, $l = -1$ and $\alpha = 0.2$.

grated to obtain the temporal component of the vector potential A_μ , however, one needs to specify the form of the coupling function V (see below). Therefore, we can at least express the invariant F as

$$F(r) = \left[\frac{Q^2}{2r^4 V^2} \right]^{\frac{1}{2s-1}}, \quad (44)$$

where the integration constant has been interpreted as an electric charge. The integration constant Q appearing in the above expression does not correspond to the standard Maxwell electric charge. Instead, in nonlinear electrodynamics it is associated with the conserved flux of the electromagnetic displacement tensor that follows from the field equations of the nonlinear electromagnetic sector. Due to the nonlinear electromagnetic coupling, this quantity does not manifest as an asymptotic gravitational charge constant associated with the vector field. To better understand this point, let us expand the radial metric potential, that is,

$$g_{rr}(r) = \left[1 + \frac{2M}{r} + \mathcal{O}\left(\frac{1}{r^2}\right) \right] \left[1 - \frac{l\alpha}{(b-2)^2 r^2} + \mathcal{O}\left(\frac{1}{r^4}\right) \right], \quad (45)$$

where we have considered $c = -2$. Therefore, one has the same asymptotic behavior as the Schwarzschild BH²

$$g_{rr}(r) = 1 + \frac{2M}{r} + \mathcal{O}\left(\frac{1}{r^2}\right), \quad (46)$$

where it is clear that there is no evidence of the scalar and vector fields for far enough distances, both represented by the parameters l and α due to the non-minimal

² Of course, a different value for the c parameter could change in principle the asymptotic behavior of the solution, and here, we took the value which guarantees flatness and stability (see below).

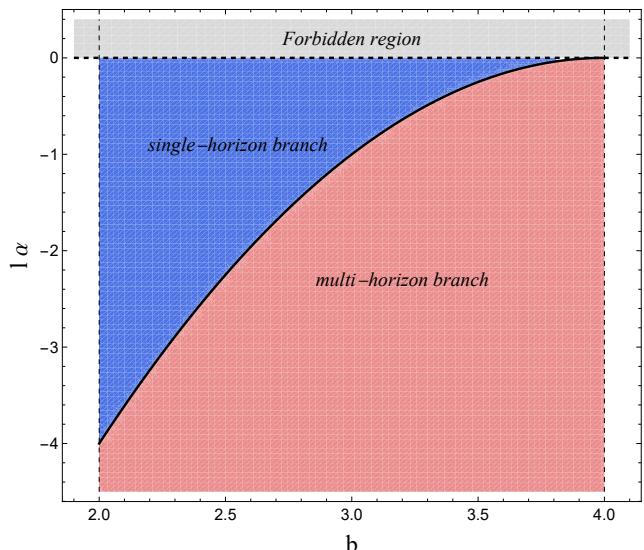


FIG. 2. Parameter-space structure of the minimally deformed solution in the $(b, l\alpha)$ plane for the representative case $M = 1$ and $c = -2$. The solid curve $l\alpha_{\text{crit}}(b) = -(4-b)^2$ separates the single-horizon branch (blue) from the multi-horizon branch (red). The dashed horizontal line $l\alpha = 0$ corresponds to the Schwarzschild limit where the deformation vanishes, while the gray region above it corresponds to $l\alpha > 0$, which lies outside the branch considered in the present analysis. The vertical dashed lines indicate the interval $2 < b < 4$ required for the regular behavior of the deformation.

coupling between them. In other words, the solution is screened by the Schwarzschild BH. Furthermore, while the action contains a nonlinear electromagnetic sector, the anisotropic closure employed to obtain the exact solution prevents a simultaneous Maxwell-canonical scalar limit. Therefore, the present geometry should be interpreted as a distinct branch rather than a continuous deformation of Einstein-scalar-Maxwell BH.

C. Explicit matter-sector reconstruction in the representative branch

Although the general system determining the scalar-vector sector does not admit a simple closed-form solution for arbitrary parameters, the situation simplifies considerably in the representative branch used throughout the numerical analysis of this work. In particular, for the choice $\{M, b, c, l, \alpha\} = \{1, 3, -2, -1, -0.2\}$, which lies inside the one-horizon region of the parameter space, the matter sector can be reconstructed explicitly.

For this branch the closure relation fixes $\{a, m, s\} = \{2, 1, 2\}$, so that the scalar-vector Lagrangian reduces to the particularly simple form

$$\mathcal{L}_m = X - F^2 V(\phi). \quad (47)$$

a. Scalar field. Using the general expression for the scalar kinetic invariant and the background metric, the

radial derivative of the scalar field becomes

$$\phi'(r)^2 = \frac{\lambda}{r[(r+1)^2 - \beta]}, \quad (48)$$

where the positive constant λ and the deformation parameter $\beta \equiv -\alpha l$ have absorbed numerical factors.

Equation (48) can be integrated exactly. Introducing the change of variable $r = T^2$, the scalar profile can be written in terms of an incomplete elliptic integral of the first kind,

$$\phi(r) = \phi_0 \pm \tilde{A}F\left(\arctan\sqrt{\frac{r}{\tilde{B}}}\middle|\tilde{C}\right), \quad (49)$$

where F denotes the elliptic integral of the first kind and the constants $(\tilde{A}, \tilde{B}, \tilde{C})$ depend only on the deformation parameter β .

This expression shows explicitly that the scalar field remains regular across the event horizon. In particular, evaluating Eq. (48) at the Schwarzschild horizon $r_H = 2$ yields

$$\phi'(r_H)^2 = \frac{\lambda}{2(9 - \beta)}, \quad (50)$$

which is finite for the allowed range $0 < \beta < 1$. Therefore the regular branch $m = 1$ eliminates the divergence that would otherwise appear in the scalar sector.

At large distances, one finds

$$\phi(r) = \phi_\infty - \frac{\kappa}{r} + \mathcal{O}(r^{-2}), \quad (51)$$

so the scalar field approaches a constant asymptotically, consistently with the asymptotic Schwarzschild behaviour of the geometry.

b. Vector sector and nonlinear coupling. The nonlinear electromagnetic equation fixes the invariant F algebraically. Combining this relation with the Einstein equations yields

$$F(r)^2 V(r) = \frac{\sigma}{r^2(r+1)^3}, \quad (52)$$

where σ absorbs numerical constants.

Solving the vector equation then determines the radial coupling function explicitly,

$$V(r) = V_0 \frac{(r+1)^9}{r^2}, \quad (53)$$

with V_0 a constant. Substituting Eq. (53) into (52) gives the electromagnetic invariant

$$|F(r)| \propto (r+1)^{-6}. \quad (54)$$

Hence, the nonlinear electromagnetic field decays rapidly at large distances, ensuring that the effective source term appearing in the gravitational equations remains asymptotically suppressed.

c. Electric potential. For a purely electric configuration $A_\mu = (A_0(r), 0, 0, 0)$ one obtains

$$A'_0(r) = \frac{\gamma}{(r+1)^2 \sqrt{5r^2 + 10r + 4}}, \quad (55)$$

where γ is proportional to the electric charge. The potential itself is therefore determined by a single quadrature.

The reconstruction above shows that the anisotropic sector generated by gravitational decoupling can be consistently interpreted as arising from a scalar field interacting with a nonlinear electromagnetic sector. The scalar profile is regular across the horizon and asymptotically constant, while the electromagnetic invariant decays sufficiently fast to preserve the asymptotic Schwarzschild structure.

Consequently, the deformation induced by the decoupler function admits a consistent matter interpretation in terms of a scalar–vector theory, rather than representing a purely effective anisotropic fluid.

D. Stability via odd and even parity criteria

Here we employ the master equations derived in [45, 46] for odd and even parity perturbation modes, obtained for the following theory

$$S = \int d^4x \sqrt{-g} \left[f_1(\phi) \frac{R}{16\pi} + f_2(\phi, X, F) \right], \quad (56)$$

where the dependency on F in the function f_2 is not necessarily linear in the Maxwell field, that is, it accepts the so-called non-linear electrodynamic forms. The action (56) corresponds to a general expression for the well-known Einstein-Maxwell-dilaton theories [6, 7].

Comparing our theory

$$S = \int d^4x \sqrt{-g} \left[\frac{R}{16\pi} + X^m - F^s V(\phi) \right] \quad (57)$$

with (56), one obtains

$$f_1(\phi) = 1, \quad f_2(\phi, X, F) = X^m - F^s V(\phi). \quad (58)$$

Thus, our proposal considers a minimal coupling between the gravitational and scalar sectors, while non-minimal coupling between the scalar and vector sectors, where in principle the vector sector corresponds to non-linear form of Maxwell interaction and the potential $V(\phi)$ is not being the usual dilatonic form.

Next, we are going to analyze under what conditions for the parameter space $\{m, s\}$, the odd and even parity master equations for stability are fulfilled.

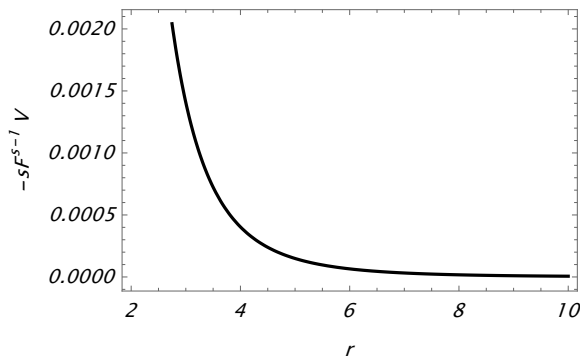


FIG. 3. Odd parity condition for stability for $M = 1$, $b = 3$, $c = -2$, $l = -1$ and $\alpha = 0.2$.

1. Odd parity constraints

The stability conditions imposed by the odd parity analysis entail in this case the satisfaction of the following inequalities

$$f_1(\phi) > 0, \quad \frac{\partial f_2(\phi, X, F)}{\partial F} > 0. \quad (59)$$

The first one is related to the ghost-free condition for the scalar fields, while the second concerns the stability under vector perturbations. In our case, $f_1(\phi) = 1$, so the first inequality is trivially satisfied. For the second condition, one gets

$$\frac{\partial f_2(\phi, X, F)}{\partial F} = -sF^{s-1}V(\phi) > 0. \quad (60)$$

In this case, the odd parity stability condition is connected with the expression given by Eq. (43). Then, to ensure stability via odd parity master conditions, expression (43) should always be positive. This fact is shown by Fig. 3 where the condition (60) is satisfied.

2. Even parity constraints

The even parity stability criterion establishes the following conditions

$$f_1(\phi) > 0, \quad 3 \left[\frac{\partial f_1(\phi)}{\partial \phi} \right]^2 + 2f_1(\phi) \frac{\partial f_2(\phi, X, F)}{\partial X} > 0. \quad (61)$$

As before, the first condition is immediately satisfied, while the second one provides

$$mX^{m-1} > 0. \quad (62)$$

It is clear that the satisfaction of the even parity stability condition is guaranteed only if $m > 0$. This condition is represented in Fig. 4.

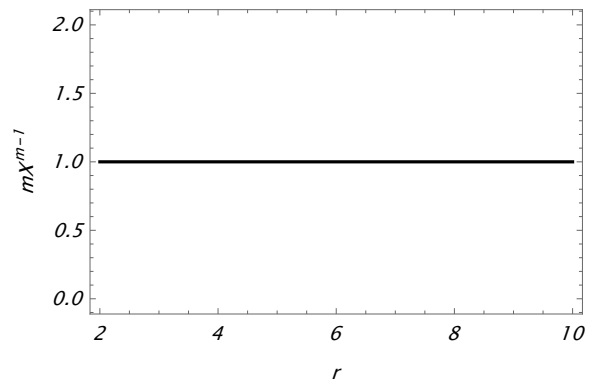


FIG. 4. Even parity condition for stability for $M = 1$, $b = 3$, $c = -2$, $l = -1$ and $\alpha = 0.2$.

IV. GEODESIC MOTION

In this section, we study the main properties of equatorial orbits around the solution described above. The geodesic motion of a test particle in a metric $g_{\mu\nu}$ is governed by the Lagrangian

$$\mathcal{L} = \frac{1}{2} g_{\mu\nu} \dot{x}^\mu \dot{x}^\nu = \frac{\epsilon}{2}, \quad (63)$$

where $\dot{x}^\mu = dx^\mu/d\tau$ being τ an affine parameter, and $\epsilon = 1$ for massive particles and $\epsilon = 0$ for photons. It is worth mentioning that, in the present analysis, we restrict ourselves to the motion of neutral test particles to isolate the purely geometrical effects associated with the MGD deformation of the radial metric component. The study of charged particle dynamics in the presence of the nonlinear electromagnetic field would require the inclusion of the Lorentz force in the equations of motion and could reveal additional dynamical features related to the scalar–vector sector. Such an analysis lies beyond the scope of the present work but represents an interesting direction for future research (see, e.g., [47])

Due to the spherical symmetry, we can restrict the particle's motion to the equatorial plane ($\theta = \pi/2$, $\dot{\theta} = 0$) without loss of generality. Besides, since the metric is independent of the coordinates t and ϕ , we have two constants of motion, namely E and L , which are the total energy and angular momentum per unit mass respectively,

$$\frac{d}{d\tau} \frac{\partial \mathcal{L}}{\partial \dot{t}} = 0 \Rightarrow \frac{\partial \mathcal{L}}{\partial \dot{t}} = g_{tt} \dot{t} = E \quad (64)$$

$$\frac{d}{d\tau} \frac{\partial \mathcal{L}}{\partial \dot{\phi}} = 0 \Rightarrow \frac{\partial \mathcal{L}}{\partial \dot{\phi}} = g_{\phi\phi} \dot{\phi} = -L. \quad (65)$$

Using Eqs. (64) and (65), we can rewrite Eq. (63) as

$$-g_{tt} g_{rr} \dot{r}^2 = E^2 - g_{tt} \left(\epsilon - \frac{L^2}{g_{\phi\phi}} \right). \quad (66)$$

Note that (66) is formally the same as the conservation

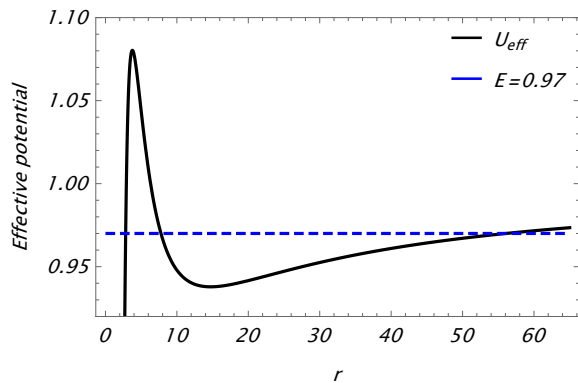


FIG. 5. Radial The effective potential versus the radial coordinate for $M = 1$, $b = 3$, $c = -2$, $\alpha = 0.2$ and $l = -1$.

equation in Newtonian mechanics with potential

$$U_{\text{eff}} = g_{tt} \left(\epsilon - \frac{L^2}{g_{\phi\phi}} \right), \quad (67)$$

which only depends on the metric functions g_{tt} and $g_{\phi\phi}$. The effective potential U_{eff} for massive particles ($\epsilon = 1$) is shown in Fig. 5. Note that a massive particle with energy E and angular momentum L has a bounded orbit whenever there are two intersection points between E^2 and U_{eff} and $E^2 > U_{\text{eff}}$ in the region between the intersections, as occurs in the Newtonian case.

To study the geodesic motion of massive particles, we can consider

$$\frac{dr}{d\tau} = \frac{dr}{d\phi} \frac{d\phi}{d\tau} = -\frac{L}{g_{\phi\phi}} \frac{dr}{d\phi}, \quad (68)$$

to rewrite Eq. (66) as

$$\frac{dr}{d\phi} = \sqrt{-\frac{g_{\phi\phi}^2}{L^2 g_{rr} g_{tt}} (E^2 - U_{\text{eff}})} \quad (69)$$

$$= \sqrt{-\frac{g_{\phi\phi}^2}{L^2 g_{rr}} \left(\frac{E^2}{g_{tt}} + \frac{L^2}{g_{\phi\phi}} - \epsilon \right)}, \quad (70)$$

from where it can be easily understood the necessity for a bound orbit to have $E^2 > U_{\text{eff}}$ such that the square root always yields real values. To solve the Eq. (69), we follow the standard procedure of Chandrasekar [48] by considering the parametrization of a bounded orbit

$$r(\chi) = \frac{\tilde{a}}{1 + \tilde{b} \cos \chi}, \quad (71)$$

where \tilde{a} and \tilde{b} are constants such that $r(0) = r_{\text{min}}$ and $r(\pi) = r_{\text{max}}$ corresponding to the periastron and the apastron respectively. Then we arrive at the differential equation

$$\frac{d\phi}{d\chi} = \frac{\tilde{a}\tilde{b}L \sin \chi}{(1 + \tilde{b} \cos \chi)^2} \sqrt{-\frac{g_{rr} g_{tt}}{g_{\phi\phi}^2} (E^2 - U_{\text{eff}})}, \quad (72)$$

that can be solved numerically. The recipe is to choose a value for E and L such that $E^2 > U_{\text{eff}}$ has a well-defined region with a minimum and maximum radius. Here we choose $E = 0.97$ and $L = 4.3$. Next, we find the values of the periastron and apastron for these particular parameters, in our case $r_{\text{min}} = 2.753$ and $r_{\text{max}} = 19.331$ from where $\tilde{a} = 4.819$ and $\tilde{b} = 0.705$. It is worth noticing that the values for r_{min} and r_{max} will be the same for all the geodesics shown in this work. This information is enough to solve Eq. (72) numerically.

Figure 6 displays three qualitatively distinct classes of timelike geodesics: bounded orbits (left panel), scattering orbits (middle panel), and plunge orbits (right panel). In all panels, the dotted black curve corresponds to the Schwarzschild solution, whereas the solid red curve represents the orbit in the scalar–vector geometry (36) for the same conserved quantities E and L , using the parameters $M = 1$, $b = 3$, $c = -2$, $\alpha = 0.2$, and $l = -1$.

Bounded orbits (left panel). Bounded trajectories oscillate between a periastron radius r_{min} and an apastron radius r_{max} . Because the effective potential U_{eff} is identical in both spacetimes—a consequence of the fact that the MGD deformation leaves g_{tt} and $g_{\phi\phi}$ unchanged—the radial motion coincides exactly in the two geometries. As a result, the values of $(r_{\text{min}}, r_{\text{max}})$ agree identically. The azimuthal motion, however, depends on the radial metric component g_{rr} through the relation

$$\frac{d\phi}{dr} \propto \sqrt{\frac{g_{\phi\phi}^2}{L^2 g_{rr} g_{tt}}} \frac{1}{\sqrt{E^2 - U_{\text{eff}}(r)}}, \quad (73)$$

and therefore differs between the two spacetimes. This produces distinct periapsis precessions: the rosette-shaped red orbit accumulates a different azimuthal angle per radial period when compared with the Schwarzschild one. The left panel thus shows that the MGD deformation breaks the exact degeneracy between the radial and azimuthal frequencies, generating a measurable change in the perihelion advance while preserving the turning points of the motion.

Scattering orbits (middle panel). The middle panel shows unbound (scattering) trajectories. For the chosen energy E , the particle comes from spatial infinity, reaches a minimum radius r_{min} —determined solely by the shape of U_{eff} and therefore identical in both metrics—and then returns to infinity. The total deflection angle,

$$\Theta = \pi - 2 \int_{r_{\text{min}}}^{\infty} \frac{d\phi}{dr} dr, \quad (74)$$

is nevertheless sensitive to the radial metric function g_{rr} . Accordingly, the red trajectory exhibits a deflection that differs from the Schwarzschild prediction, despite the fact that the effective potential and the asymptotic structure are the same. This constitutes a clean, coordinate-invariant imprint of the MGD deformation on dynamical observables.

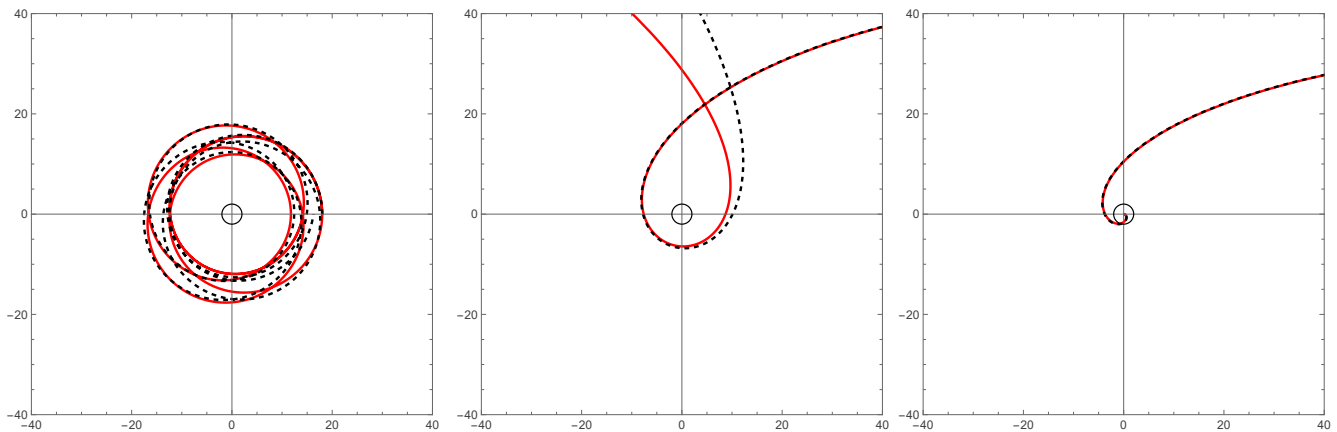


FIG. 6. **Left panel:** Bounded orbits. **Middle panel:** Scattering orbit. **Right panel:** Plunge orbit. For these plots we consider $M = 1$, $b = 3$, $c = -2$, $\alpha = 0.2$ and $l = -1$. The black line corresponds to the Schwarzschild BH, and the blue one to the model (36).

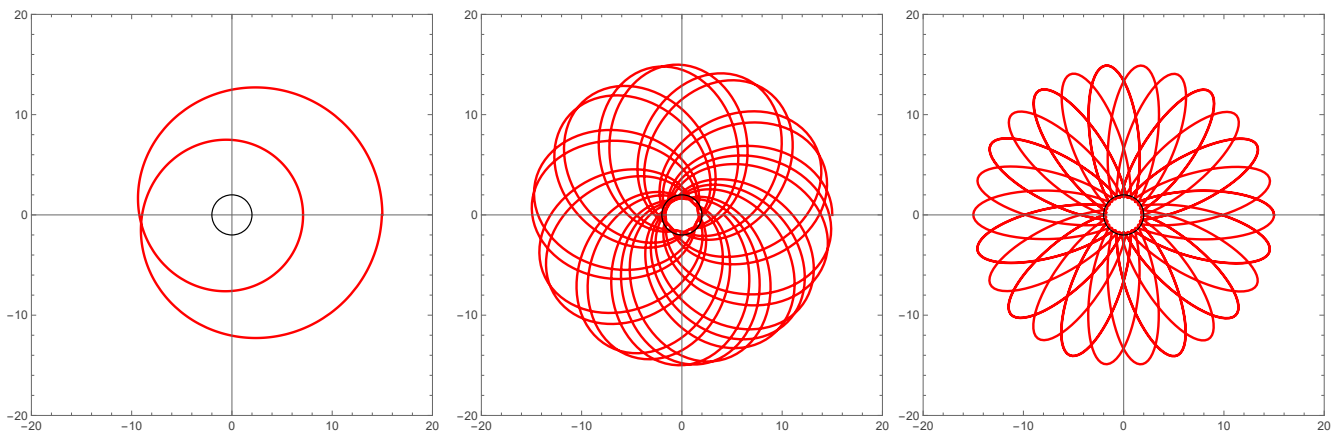


FIG. 7. Bounded orbits for a massive particle moving in the equatorial plane for different values of the parameter l .

Plunge orbits (right panel). The right panel now illustrates plunge trajectories for which the particle has no outer turning point: once it crosses the maximum of the effective potential, it inevitably falls toward the horizon. In this case, the red and black curves *coincide almost perfectly throughout the entire trajectory*. This complete overlap reflects the fact that plunging trajectories probe only the radial inequality $E^2 > U_{\text{eff}}(r)$ and do not undergo oscillatory motion. Since U_{eff} and g_{tt} are identical in the two geometries, the combination

$$E^2 - U_{\text{eff}}(r) \quad (75)$$

that governs the monotonic radial fall is the same. Although in principle the accumulated azimuthal angle before crossing the horizon depends on g_{rr} , for plunging trajectories this effect is too small to produce a visible separation of the curves. Consequently, the plunge orbits in Figure 6 are practically indistinguishable from their Schwarzschild counterparts, in stark contrast with the bounded and scattering cases.

Figure 7 focuses on bounded orbits and illustrates how

the orbital shape varies with the constant parameter l . Because neither the position of the horizon nor the effective potential depends on l , the periastron and apastron radii remain fixed for all curves. The only quantity affected is the radial component of the metric, g_{rr} , which becomes increasingly deformed as $|l|$ grows (for $l < 0$ in the examples shown). This induces a systematic variation of the periastron precession: larger values of $|l|$ lead to greater departures from the Schwarzschild rosette, while $l \rightarrow 0$ (or $\alpha \rightarrow 0$) smoothly recovers the pure Schwarzschild dynamics.

In summary, Figures 6 and 7 demonstrate that minimally deformed black holes obtained via gravitational decoupling share the same global orbit classification and the same radial turning points as Schwarzschild, but exhibit quantitative and observable differences in the periastron precession and scattering angle. Plunge orbits constitute the only exception: due to their strictly monotonic radial behavior, they are effectively insensitive to the MGD corrections and therefore lie on top of the Schwarzschild results.

V. THERMODYNAMIC ASPECTS

In this section, we present a strengthened and conceptually sharpened analysis of the thermodynamics associated with the minimally deformed Schwarzschild geometry introduced earlier.

As the event horizon remains fixed at $r_H = 2M$, the parameter M can be formally identified as the BH mass. Although the functional form of g_{tt} coincides with the Schwarzschild one, the deformation encoded in f fundamentally modifies the redshift properties near the horizon and is responsible for the polymer-inspired deviations in all thermodynamic quantities. The parameters α and l therefore act as control parameters, and the classical limit is easily recovered as $\alpha \rightarrow 0$.

The Hawking temperature follows directly from the surface gravity associated with the timelike Killing field. Using the general expression [49]

$$T_H = \frac{1}{4\pi} \sqrt{\partial_r g_{tt}(r_H) \partial_r g^{rr}(r_H)}, \quad (76)$$

One obtains

$$T_H = \frac{1}{4\pi r_H} \sqrt{\frac{2^c + l\alpha (br_H)^c}{2^c}}. \quad (77)$$

Thus, the temperature is universally suppressed relative to the Schwarzschild value $T_0 = 1/(4\pi r_H)$. This suppression is not a small correction but a structural consequence of the polymerized radial sector. The small expansion of $\alpha \rightarrow 0$ of (77) yields

$$T_H = T_0 \left[1 + \frac{(br_H)^c l\alpha}{2^{c+1}} \right] + \mathcal{O}(\alpha^2), \quad (78)$$

showing explicitly the monotonic decrease of T_H when considering $l\alpha < 0$, see left panel in Fig. 8.

The entropy follows from

$$dS = \frac{dM}{T_H}. \quad (79)$$

Using (77), one obtains after integration

$$S = \pi r_H^2 {}_2F_1 \left[\frac{1}{2}, \frac{2}{c}, \frac{2+c}{c}, -\frac{(br_H)^c l\alpha}{2^c} \right]. \quad (80)$$

Hence, the entropy is modified by the effects of MGD. The increase in S reflects the fact that the polymer deformation effectively enlarges the horizon area by a multiplicative renormalization of the radial measure. Expanding (80) for small $l\alpha$ produces

$$S = S_0 \left[1 - \frac{2^{-c} (br_H)^c l\alpha}{2+c} + \mathcal{O}(\alpha^2) \right], \quad (81)$$

with $S_0 = \pi r_H^2$ the classical Bekenstein–Hawking entropy. As $l\alpha < 0$, the modifications to the entropy do

not damage its increasing behavior, as depicted in the middle panel in Fig. 8.

Now, the heat capacity follows the standard definition

$$C_v = T_H \left(\frac{\partial S}{\partial T_H} \right) = T_H \frac{\left(\frac{\partial S}{\partial r_H} \right)}{\left(\frac{\partial T_H}{\partial r_H} \right)}. \quad (82)$$

Carrying out the computation with (77) and (80) leads to the exact result

$$C_v = -\frac{2^{2+c} \pi r_H^2 \sqrt{1 + 2^{-c} (br_H)^c l\alpha}}{2^{1+c} + (c-2)(br_H)^c l\alpha}. \quad (83)$$

This quantity remains *negative*, confirming that the BH is thermodynamically unstable. In other words, polymerization sharpens the runaway evaporation behavior instead of stabilizing BH in the canonical ensemble.

The Gibbs free energy provides additional thermodynamic information. However, we first need to compute the ADM mass for this model before obtaining the free energy. So, the ADM mass is defined by [50]

$$M_{\text{ADM}} = \frac{1}{16\pi} \lim_{r \rightarrow \infty} \int \sum_{i,j=1}^3 (g_{ij,i} - g_{ii,j}) n^j dA \quad (84)$$

where the integral is over a sphere of constant radius

$$r = \sqrt{(x^1)^2 + (x^2)^2 + (x^3)^2}, \quad n^j = x^j/r, \quad (85)$$

and dA the surface element. Here, the spatial component of the metric for large values of r is given by

$$g_{ij} = \left[1 + \frac{2M}{r} + \mathcal{O}\left(\frac{1}{r^2}\right) \right] \delta_{ij}. \quad (86)$$

Therefore,

$$g_{ij,i} - g_{ii,j} = -2\partial_j \left[\frac{2M}{r} + \mathcal{O}\left(\frac{1}{r^2}\right) \right]. \quad (87)$$

So, putting together (84) and (87) one obtains

$$M_{\text{ADM}} = M. \quad (88)$$

This is a non-trivial result, because some non-Schwarzschild BH such as the one reported by [51] in the framework of quantum gravity theory, has an ADM mass which is not the parameter M in the metric [52].

Now, the Gibbs free energy is given by

$$G = M_{\text{ADM}} - T_H S. \quad (89)$$

For the present case, G has the following expression

$$G = \frac{r_H}{4} \left[1 - \frac{(br_H)^c l\alpha}{2^c} \right] {}_2F_1 \left[\frac{1}{2}, \frac{2}{c}, \frac{2+c}{c}, -\frac{(br_H)^c l\alpha}{2^c} \right], \quad (90)$$

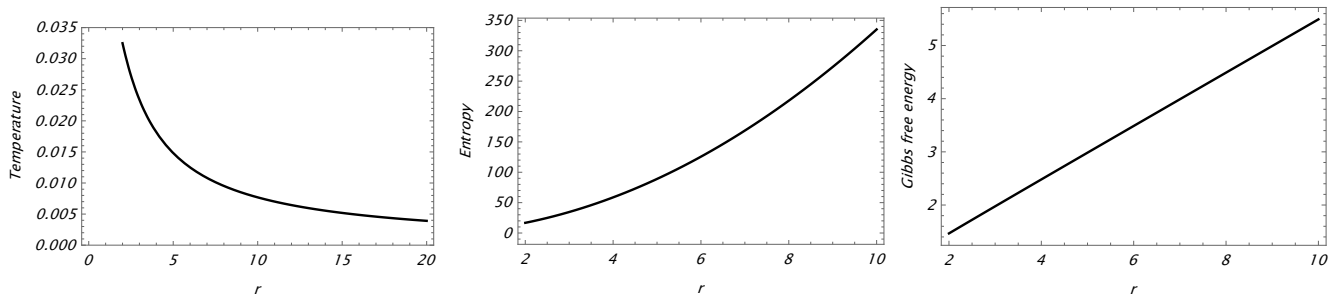


FIG. 8. **Left panel:** Temperature. **Middle:** Entropy. **Right panel:** Gibbs free energy. For these plots we consider $M = 1$, $b = 3$, $c = -2$, $\alpha = 0.2$ and $l = -1$.

which differs markedly from the Schwarzschild expression. Its trend is shown by the right panel in Fig. 8, corroborating the thermodynamical instability of the model.

Next, expanding for a small α leads to

$$G = G_0 - \frac{2^{-3-c} c r_H (b r_H)^c}{2+c} l \alpha + \mathcal{O}(\alpha^2), \quad (91)$$

with $G_0 \equiv r_H/4$.

The thermodynamic portrait that emerges is therefore unambiguous, the polymer parameter $l\alpha$ acts coherently across all quantities by lowering the temperature, increasing the entropy and heat capacity in magnitude, and modifying the Gibbs energy in a qualitatively new way that cannot be reproduced by a simple rescaling of the Schwarzschild mass. Every correction vanishes smoothly in the limit $\alpha \rightarrow 0$, but for any finite α and l the deviations are systematic.

VI. CONCLUSIONS

In this work, we have constructed and analyzed a new class of static and spherically symmetric BH geometries arising from a scalar-vector sector governed by a non-linear electrodynamic interaction, minimally coupled to gravity but incorporated into the geometry through the Minimal Geometric Deformation (MGD) approach. Starting from the Schwarzschild solution as the seed geometry and introducing a general algebraic relation among the components of the decoupling tensor $\theta_{\mu\nu}$, we derived closed and fully analytical expressions for the decoupler function f and for the resulting minimally deformed metric. This provides, to our knowledge, the first exact non-Schwarzschild BH sourced by a genuine scalar-vector system within the framework of GD.

A crucial outcome of our construction is that the deformation is encoded entirely in the radial sector of the metric, leaving g_{tt} unchanged and thus preserving the location of the Schwarzschild horizon at $r_H = 2M$. We have shown that the interplay between the parameters (a, b) of the effective equation of state, the exponents (m, s) of the scalar and vector sectors, and the MGD constants (l, α) determines whether the deformation maintains a healthy Lorentzian signature. By analyzing the

roots of g^{rr} we established sharp conditions that ensure that no additional horizons or signature changes appear, thus producing a well-defined causal structure consistent with asymptotic flatness.

A second major contribution of this work is the systematic study of stability under both odd and even-parity perturbations using the master equations developed for the most general scalar-vector-tensor theory. We demonstrated that the model satisfies all ghost-free and gradient-stability requirements provided that the exponents (m, s) lie within the regions dictated by Eqs. (60) and (62). In particular, the odd-parity sector imposes a non-trivial positivity condition on the combination $-sF^{s-1}V(\phi)$, which we explicitly verified, and the even-parity sector requires $m > 0$, ensuring that the effective kinetic term remains positive. The combined analysis thus confirms that our BH solution is perturbatively stable for a physically meaningful subset of the parameter space.

To further assess the physical viability of the model, we examined the geodesic structure of the resulting spacetime. Since the deformation preserves g_{tt} and $g_{\varphi\varphi}$, the effective potential for massive particles remains identical to the Schwarzschild one, and therefore the radial turning points of bound, scattering, and plunge orbits are unchanged. However, the deformation of the radial component g_{rr} modifies the relation between the radial and angular frequencies. This leads to observable differences in periastron precession, deflection angles, and plunge dynamics, as illustrated in Figs. 6 and 7. The MGD parameter α thus serves as a continuous control of how strongly the scalar-vector sector distorts orbital motion, while the global qualitative behavior remains close to Schwarzschild.

Finally, we provided an exhaustive thermodynamic analysis of the deformed geometry. By computing the surface gravity at the unchanged horizon $r_H = 2M$, we found a universal suppression of the Hawking temperature with respect to Schwarzschild, controlled by the effective polymer-like corrections induced by f . The entropy, derived from the first law, exhibits a non-trivial hypergeometric dependence on the deformation parameters, reflecting a multiplicative renormalization of the radial measure at the horizon. The heat capacity remains

negative, preserving the well-known thermodynamic instability of the Schwarzschild BH, and the Gibbs free energy receives some new contributions too. In this context, it is worth mentioning that the ADM mass of the model coincides with the mass parameter M . This occurs because the scalar–vector sector does not generate an independent asymptotic charge. Instead, it induces a purely radial geometric deformation, preserving the Schwarzschild-like temporal potential and therefore the ADM mass. This suggests that the scalar and vector fields exhibit a stealth-like behavior. This means that physically, the stealth behavior implies that the scalar and vector fields possess non-trivial energy–momentum and actively curve the spacetime, yet they do not generate an independent asymptotic gravitational charge. As a result, the external geometry remains Schwarzschild-like at large distances, making the fields effectively invisible.

An additional result obtained in this work concerns the explicit reconstruction of the matter sector supporting the geometry. Although the general scalar–vector system arising from the decoupling equations does not admit a simple closed-form solution for arbitrary param-

eters, we have shown that in the representative branch used in our analysis, the matter sector can be determined explicitly. In particular, the scalar field profile can be obtained in closed form in terms of elliptic functions, while the nonlinear electromagnetic invariant and the coupling function $V(r)$ are fully determined analytically. This reconstruction demonstrates that the anisotropic source generated through gravitational decoupling admits a consistent interpretation in terms of a scalar field interacting with a nonlinear electromagnetic sector rather than representing a purely effective fluid description.

Taken together, these results show that the MGD framework, when coupled with a scalar–vector sector of the type considered here, provides a powerful and analytically tractable method for generating new BH solutions with controlled departures from Schwarzschild while preserving stability, asymptotic flatness, and a single event horizon. The model developed in this paper, therefore, expands the known landscape of BHs supported by non-linear electrodynamics and scalar fields, and offers a fertile ground for the study of modified geodesic phenomenology, near-horizon corrections, and effective polymer-like deformations within classical gravity.

-
- [1] B. P. Abbott, et al., Observation of Gravitational Waves from a Binary Black Hole Merger, *Phys. Rev. Lett.* 116 (6) (2016) 061102. [arXiv:1602.03837](#), [doi:10.1103/PhysRevLett.116.061102](#).
- [2] R. e. a. Abbott, Gwtc-3: Compact binary coalescences observed during the second part of the third observing run, *Phys. Rev. X* 11 (2021) 021053. [arXiv:2111.03606](#), [doi:10.1103/PhysRevX.11.021053](#).
- [3] K. e. a. Akiyama, First m87 event horizon telescope results. i. the shadow of the supermassive black hole, *Astrophys. J. Lett.* 875 (1) (2019) L1. [doi:10.3847/2041-8213/ab0ec7](#).
- [4] K. e. a. Akiyama, First m87 event horizon telescope results. iv. imaging the central supermassive black hole, *Astrophys. J. Lett.* 875 (1) (2019) L4. [doi:10.3847/2041-8213/ab0f43](#).
- [5] K. e. a. Akiyama, First sagittarius a* event horizon telescope results. i. the shadow of the supermassive black hole, *Astrophys. J. Lett.* 930 (2) (2022) L12. [doi:10.3847/2041-8213/ac6674](#).
- [6] G. W. Gibbons, K.-i. Maeda, Black Holes and Membranes in Higher Dimensional Theories with Dilaton Fields, *Nucl. Phys. B* 298 (1988) 741–775. [doi:10.1016/0550-3213\(88\)90006-5](#).
- [7] D. Garfinkle, G. T. Horowitz, A. Strominger, Charged black holes in string theory, *Phys. Rev. D* 43 (1991) 3140, [Erratum: *Phys.Rev.D* 45, 3888 (1992)]. [doi:10.1103/PhysRevD.43.3140](#).
- [8] L. Heisenberg, Generalized proca theories, *JCAP* 05 (2014) 015. [arXiv:1402.7026](#), [doi:10.1088/1475-7516/2014/05/015](#).
- [9] A. De Felice, L. Heisenberg, S. Tsujikawa, Observational constraints on generalized proca theories, *Phys. Rev. D* 94 (2016) 044024. [arXiv:1605.05066](#), [doi:10.1103/PhysRevD.94.044024](#).
- [10] S. H. Hendi, Asymptotic reissner–nordström black holes, *Annals Phys.* 333 (2013) 282–290. [arXiv:1202.1718](#), [doi:10.1016/j.aop.2013.02.008](#).
- [11] K. A. Bronnikov, Regular magnetic black holes and monopoles from nonlinear electrodynamics, *Phys. Rev. D* 63 (2001) 044005. [doi:10.1103/PhysRevD.63.044005](#).
- [12] R. Kase, S. Tsujikawa, Dark energy in horndeski theories after gw170817, *Int. J. Mod. Phys. D* 28 (2019) 1942005. [arXiv:1809.08735](#), [doi:10.1142/S0218271819420057](#).
- [13] E. Babichev, C. Charmousis, G. Esposito-Farèse, Charge without charge: Black hole solutions in scalar–tensor gravity, *Phys. Rev. Lett.* 116 (2016) 171101. [arXiv:1512.04098](#), [doi:10.1103/PhysRevLett.116.171101](#).
- [14] J. Ovalle, Decoupling gravitational sources in general relativity: from perfect to anisotropic fluids, *Phys. Rev. D* 95 (10) (2017) 104019. [doi:10.1103/PhysRevD.95.104019](#).
- [15] J. Ovalle, R. Casadio, R. da Rocha, A. Sotomayor, Z. Stuchlik, Einstein-Klein-Gordon system by gravitational decoupling, *EPL* 124 (2) (2018) 20004. [arXiv:1811.08559](#), [doi:10.1209/0295-5075/124/20004](#).
- [16] E. Contreras, A. Rincón, P. Bargueño, A general interior anisotropic solution for a BTZ vacuum in the context of the Minimal Geometric Deformation decoupling approach, *Eur. Phys. J. C* 79 (3) (2019) 216. [arXiv:1902.02033](#), [doi:10.1140/epjc/s10052-019-6749-9](#).
- [17] R. da Rocha, Minimal geometric deformation and holographic principles, *Phys. Rev. D* 102 (2020) 024011. [doi:10.1103/PhysRevD.102.024011](#).
- [18] Y. Heydarzade, M. Misyura, V. Vertogradov, Hairy Kiselev black hole solutions, *Phys. Rev. D* 108 (4) (2023) 044073. [arXiv:2307.04556](#), [doi:10.1103/PhysRevD.108.044073](#).

- [19] J. Ovalle, R. Casadio, R. d. Rocha, A. Sotomayor, Z. Stuchlik, Black holes by gravitational decoupling, *Eur. Phys. J. C* 78 (11) (2018) 960. [arXiv:1804.03468](#), [doi:10.1140/epjc/s10052-018-6450-4](#).
- [20] R. T. Cavalcanti, K. d. S. Alves, J. M. Hoff da Silva, Near-Horizon Thermodynamics of Hairy Black Holes from Gravitational Decoupling, *Universe* 8 (7) (2022) 363. [arXiv:2207.03995](#), [doi:10.3390/universe8070363](#).
- [21] R. T. Cavalcanti, R. C. de Paiva, R. da Rocha, Echoes of the gravitational decoupling: scalar perturbations and quasinormal modes of hairy black holes, *Eur. Phys. J. Plus* 137 (10) (2022) 1185. [arXiv:2203.08740](#), [doi:10.1140/epjp/s13360-022-03407-x](#).
- [22] P. Meert, R. da Rocha, Gravitational decoupling, hairy black holes and conformal anomalies, *Eur. Phys. J. C* 82 (2) (2022) 175. [arXiv:2109.06289](#), [doi:10.1140/epjc/s10052-022-10121-6](#).
- [23] J. Sultana, Gravitational Decoupling in Higher Order Theories, *Symmetry* 13 (9) (2021) 1598. [doi:10.3390/sym13091598](#).
- [24] J. Ovalle, R. Casadio, E. Contreras, A. Sotomayor, Hairy black holes by gravitational decoupling, *Phys. Dark Univ.* 31 (2021) 100744. [arXiv:2006.06735](#), [doi:10.1016/j.dark.2020.100744](#).
- [25] R. a. da Rocha, A. A. Tomaz, MGD-decoupled black holes, anisotropic fluids and holographic entanglement entropy, *Eur. Phys. J. C* 80 (9) (2020) 857. [arXiv:2005.02980](#), [doi:10.1140/epjc/s10052-020-8414-8](#).
- [26] A. Fernandes-Silva, A. J. Ferreira-Martins, R. da Rocha, Extended quantum portrait of MGD black holes and information entropy, *Phys. Lett. B* 791 (2019) 323–330. [arXiv:1901.07492](#), [doi:10.1016/j.physletb.2019.03.010](#).
- [27] R. Casadio, A. Giusti, J. Ovalle, Quantum Reissner-Nordström geometry: Singularity and Cauchy horizon, *Phys. Rev. D* 105 (12) (2022) 124026. [arXiv:2203.03252](#), [doi:10.1103/PhysRevD.105.124026](#).
- [28] J. Ovalle, Warped vacuum energy by black holes, *Eur. Phys. J. C* 82 (2) (2022) 170. [arXiv:2202.12037](#), [doi:10.1140/epjc/s10052-022-10094-6](#).
- [29] M. Estrada, Gravitational Decoupling algorithm modifies the value of the conserved charges and thermodynamics properties in Lovelock Unique Vacuum theory, *Annals Phys.* 439 (2022) 168792. [arXiv:2106.02166](#), [doi:10.1016/j.aop.2022.168792](#).
- [30] J. Ovalle, R. Casadio, A. Giusti, Regular hairy black holes through Minkowski deformation, *Phys. Lett. B* 844 (2023) 138085. [arXiv:2304.03263](#), [doi:10.1016/j.physletb.2023.138085](#).
- [31] C.-M. Zhang, M. Zhang, D.-C. Zou, Gravitational decoupling for hairy black holes in asymptotic AdS spacetimes, *Chin. Phys. C* 47 (1) (2023) 015106. [arXiv:2208.06830](#), [doi:10.1088/1674-1137/ac9b2c](#).
- [32] M. R. Khosravipoor, M. Farhoudi, Thermodynamics of deformed AdS-Schwarzschild black hole, *Eur. Phys. J. C* 83 (11) (2023) 1045. [arXiv:2311.02456](#), [doi:10.1140/epjc/s10052-023-12222-2](#).
- [33] E. Contreras, J. Ovalle, R. Casadio, Gravitational decoupling for axially symmetric systems and rotating black holes, *Phys. Rev. D* 103 (4) (2021) 044020. [arXiv:2101.08569](#), [doi:10.1103/PhysRevD.103.044020](#).
- [34] A. Ramos, C. Arias, R. Avalos, E. Contreras, Geodesic motion around hairy black holes, *Ann. Phys.* 431 (2021) 168557. [arXiv:2107.01146](#), [doi:10.1016/j.aop.2021.168557](#).
- [35] J. Ovalle, E. Contreras, Z. Stuchlik, Kerr–de Sitter black hole revisited, *Phys. Rev. D* 103 (8) (2021) 084016. [arXiv:2104.06359](#), [doi:10.1103/PhysRevD.103.084016](#).
- [36] P. J. Arias, P. Bargueño, E. Contreras, E. Fuenmayor, 2 + 1 Einstein-Klein-Gordon black holes by gravitational decoupling, *Astronomy* 1 (1) (2022) 2–14. [arXiv:2203.00661](#), [doi:10.3390/astronomy1010002](#).
- [37] R. Avalos, P. Bargueño, E. Contreras, A Static and Spherically Symmetric Hairy Black Hole in the Framework of the Gravitational Decoupling, *Fortsch. Phys.* 71 (4-5) (2023) 2200171. [arXiv:2303.04119](#), [doi:10.1002/prop.202200171](#).
- [38] R. Avalos, E. Contreras, Quasi normal modes of hairy black holes at higher-order WKB approach, *Eur. Phys. J. C* 83 (2) (2023) 155. [arXiv:2302.09148](#), [doi:10.1140/epjc/s10052-023-11288-2](#).
- [39] J. Ovalle, Black holes without Cauchy horizons and integrable singularities, *Phys. Rev. D* 107 (10) (2023) 104005. [arXiv:2305.00030](#), [doi:10.1103/PhysRevD.107.104005](#).
- [40] R. Casadio, A. Giusti, J. Ovalle, Quantum rotating black holes, *JHEP* 05 (2023) 118. [arXiv:2303.02713](#), [doi:10.1007/JHEP05\(2023\)118](#).
- [41] E. Contreras, P. Bargueño, Minimal Geometric Deformation in asymptotically (A-)dS space-times and the isotropic sector for a polytropic black hole, *Eur. Phys. J. C* 78 (12) (2018) 985. [arXiv:1809.09820](#), [doi:10.1140/epjc/s10052-018-6472-y](#).
- [42] M. Estrada, R. Prado, A note of the first law of thermodynamics by gravitational decoupling, *Eur. Phys. J. C* 80 (8) (2020) 799. [arXiv:2003.13168](#), [doi:10.1140/epjc/s10052-020-8315-x](#).
- [43] J. Ovalle, R. Casadio, R. da Rocha, A. Sotomayor, Anisotropic solutions by gravitational decoupling, *Eur. Phys. J. C* 78 (2) (2018) 122. [arXiv:1708.00407](#), [doi:10.1140/epjc/s10052-018-5606-6](#).
- [44] M. Dehghani, M. R. Setare, Dilaton black holes with power law electrodynamics, *Phys. Rev. D* 100 (4) (2019) 044022. [arXiv:1906.11063](#), [doi:10.1103/PhysRevD.100.044022](#).
- [45] R. Gannouji, Y. R. Baez, Stability of generalized Einstein-Maxwell-scalar black holes, *JHEP* 02 (2022) 020. [arXiv:2112.00109](#), [doi:10.1007/JHEP02\(2022\)020](#).
- [46] Y. R. Baez, M. Gonzalez-Espinoza, Odd-parity perturbations in the most general scalar–vector–tensor theory, *Class. Quant. Grav.* 40 (8) (2023) 085017. [arXiv:2209.07555](#), [doi:10.1088/1361-6382/acc50d](#).
- [47] Z. Stuchlík, M. Kološ, J. Kovář, P. Slaný, A. Tursunov, Influence of Cosmic Repulsion and Magnetic Fields on Accretion Disks Rotating around Kerr Black Holes, *Universe* 6 (2) (2020) 26. [doi:10.3390/universe6020026](#).
- [48] S. Chandrasekhar, *The Mathematical Theory of Black Holes*, Oxford University Press, Inc, 1992.
- [49] M. Angheben, M. Nadalini, L. Vanzo, S. Zerbini, Hawking radiation as tunneling for extremal and rotating black holes, *JHEP* 05 (2005) 014. [arXiv:hep-th/0503081](#), [doi:10.1088/1126-6708/2005/05/014](#).
- [50] R. M. Wald, *General Relativity*, Chicago Univ. Pr., Chicago, USA, 1984. [doi:10.7208/chicago/9780226870373.001.0001](#).

- [51] A. Alonso-Bardaji, D. Brizuela, R. Vera, An effective model for the quantum Schwarzschild black hole, *Phys. Lett. B* 829 (2022) 137075. doi:10.1016/j.physletb.2022.137075.
- [52] L. Balart, G. Panotopoulos, Á. Rincón, Thermodynamics of the quantum Schwarzschild black hole, *Eur. Phys. J. Plus* 139 (5) (2024) 416. doi:10.1140/epjp/s13360-024-05216-w.